



Modeling $\Delta^{14}\text{CO}_2$ for Western Europe

D. Bozhinova et al.

Simulating the integrated $\Delta^{14}\text{CO}_2$ signature from anthropogenic emissions over Western Europe

D. Bozhinova¹, M. K. van der Molen¹, M. C. Krol^{1,2}, S. van der Laan³,
H. A. J. Meijer³, and W. Peters¹

¹Meteorology and Air Quality Group, Wageningen University, Wageningen, the Netherlands

²Institute for Marine and Atmospheric Research Utrecht, Utrecht, the Netherlands

³Centre for Isotope Research, University of Groningen, Groningen, the Netherlands

Received: 7 November 2013 – Accepted: 8 November 2013 – Published: 21 November 2013

Correspondence to: D. Bozhinova (denica.bozhinova@wur.nl)

Published by Copernicus Publications on behalf of the European Geosciences Union.

Title Page

Abstract

Introduction

Conclusions

References

Tables

Figures

◀

▶

◀

▶

Back

Close

Full Screen / Esc

Printer-friendly Version

Interactive Discussion



Abstract

Radiocarbon dioxide ($^{14}\text{CO}_2$, reported in $\Delta^{14}\text{CO}_2$) can be used to determine the fossil fuel CO_2 addition to the atmosphere, since fossil fuel CO_2 no longer contains any ^{14}C . After release of CO_2 at the source, atmospheric transport causes dilution of strong local signals into the background and detectable gradients of $\Delta^{14}\text{CO}_2$ only remain in areas with high fossil fuel emissions. This fossil fuel signal can moreover be partially masked by the enriching effect that anthropogenic emissions of $^{14}\text{CO}_2$ from the nuclear industry have on the atmospheric $\Delta^{14}\text{CO}_2$ signature. In this paper, we investigate the regional gradients in $^{14}\text{CO}_2$ over the European continent and quantify the effect of the emissions from nuclear industry. We simulate the emissions of fossil fuel CO_2 and nuclear $^{14}\text{CO}_2$ for Western Europe for a period covering 6 months in 2008 and their transport using the Weather Research and Forecast model (WRF-Chem). We evaluate the expected CO_2 gradients and the resulting $\Delta^{14}\text{CO}_2$ in simulated integrated air samples over this period, as well as in simulated plant samples.

We find that the average gradients of fossil fuel CO_2 in the lower 1200 m of the atmosphere are close to 15 ppm at a 12 km \times 12 km horizontal resolution. The nuclear influence on $\Delta^{14}\text{CO}_2$ signatures varies considerably over the domain and for large areas in France and UK it can range from 20 % to more than 500 % of the influence of fossil fuel emissions. Our simulations suggest that the resulting gradients in $\Delta^{14}\text{CO}_2$ are well captured in plant samples, but due to their time-varying uptake of CO_2 their signature can be different with over 3 % from the atmospheric samples in some regions. We conclude that the framework presented will be well-suited for the interpretation of actual air and plant $^{14}\text{CO}_2$ samples.

1 Introduction

The magnitude of anthropogenic fossil fuel CO_2 emissions is relatively well known on the global scale (Raupach et al., 2007; Friedlingstein et al., 2010) as bottom-up inven-

30612

ACPD

13, 30611–30652, 2013

Modeling $\Delta^{14}\text{CO}_2$ for Western Europe

D. Bozhinova et al.

Title Page

Abstract

Introduction

Conclusions

References

Tables

Figures

◀

▶

◀

▶

Back

Close

Full Screen / Esc

Printer-friendly Version

Interactive Discussion



Modeling $\Delta^{14}\text{CO}_2$ for
Western Europe

D. Bozhinova et al.

Title Page

Abstract

Introduction

Conclusions

References

Tables

Figures

◀

▶

◀

▶

Back

Close

Full Screen / Esc

Printer-friendly Version

Interactive Discussion



–5730 ± 40 yr (Godwin, 1962). This typically applies only to carbon in fossil reservoirs, as other carbon reservoirs are continuously supplied with fresh ^{14}C from exchange with the atmosphere where $^{14}\text{CO}_2$ is produced in the stratosphere (Libby, 1946; Anderson et al., 1947). In the natural carbon balance this ^{14}C would cycle through the atmospheric, biospheric, and oceanic reservoir until it decays. But very large anthropogenic disturbances on this natural cycle come specifically from (a) large scale burning of very old and ^{14}C depleted carbon from fossil reservoirs, the “Suess effect” (Suess, 1955; Levin et al., 1980), and (b) production of highly enriched ^{14}C in CO_2 such as from nuclear bomb tests (Nydal, 1968), or some methods of nuclear power production (McCartney and Baxter, 1988a, b). Samples of $^{14}\text{CO}_2$ taken from the atmosphere, but also from the oceans and biosphere that exchange with it, consistently show their dominant influence on the $^{14}\text{CO}_2$ budget of the past decades (e.g.: Levin et al., 1989; Meijer et al., 1996; Nydal and Gislefoss, 1996; Levin and Heshaimer, 2000; Randerson et al., 2002; Naegler and Levin, 2006; Levin et al., 2010; Graven et al., 2012a, b).

Monitoring of atmospheric $^{14}\text{CO}_2$ is done through several methods. One commonly applied approach is by absorption of gaseous CO_2 into a sodium hydroxide solution from which the carbon content is extracted and converted into a graphite target for $^{14}\text{C}/\text{C}$ analysis either by radioactive decay counters, or accelerator mass spectrometry. The air flowing into the solution typically integrates the sampling time over days, weeks, or even longer time periods. This is different from an air sample collected in a flask, which is filled within less than a minute and thus representative of a much smaller atmospheric time-window. At the other end of the time spectrum is the use of plants to sample $^{14}\text{C}/\text{C}$ ratios in the atmosphere through their photosynthetic fixation of atmospheric CO_2 . Depending on the species these integrate over sampling windows of a full growing season (annual crops, fruits – Shibata et al., 2005; Hsueh et al., 2007; Palstra et al., 2008; Riley et al., 2008; Wang et al., 2013) or longer (trees, tree-rings – Suess, 1955; Stuiver and Quay, 1981; Wang et al., 2012).

An effective monitoring strategy for fossil fuel emissions is likely to take advantage of all methods available to collect ^{14}C samples, and combine these with high resolution

Modeling $\Delta^{14}\text{CO}_2$ for
Western Europe

D. Bozhinova et al.

Title Page

Abstract

Introduction

Conclusions

References

Tables

Figures

◀

▶

◀

▶

Back

Close

Full Screen / Esc

Printer-friendly Version

Interactive Discussion



monitoring of related gases (e.g. CO, SF₆). Levin and Karstens (2007), van der Laan et al. (2010) and Vogel et al. (2010) already demonstrated the viability of a monitoring method in which observed CO/CO₂ ratios are periodically calibrated with ¹⁴CO₂ to estimate fossil fuel emissions at high temporal resolutions. More recently, this strategy was also employed by Lopez et al. (2013), where additionally the CO₂/NO_x ratios were used to estimate fossil fuel derived CO₂ from continuous CO and NO_x observations in Paris. Turnbull et al. (2011) showed for the city of Sacramento, that using a combination of $\Delta^{14}\text{CO}_2$ and CO observations can reveal structural detail in CO₂ from fossil fuel and biospheric sources that cannot be obtained by CO₂ measurements alone. van der Laan et al. (2010) and recently Vogel et al. (2013) showed that the agreement between fossil fuel CO₂ modeled estimates with observations of ¹⁴C-corrected CO can be further improved by including ²²²Rn as a tracer for the vertical mixing. Finally, Hsueh et al. (2007) and Riley et al. (2008) used ¹⁴C/C ratios in corn leaves and C3 grasses to reveal fossil fuel emission patterns on city, state, and national scales. Given so many different methods to use ¹⁴C in monitoring strategies, its increasing accuracy, reduction in required sample size, and decreasing costs, it is likely that this tracer will play a more important role in the future of the carbon observing network.

Obviously, the quantitative estimation of fossil fuel emissions from all of the ¹⁴C-based monitoring strategies above requires different methods and emphasizes different terms in the ¹⁴CO₂ budget. For example, interpretation of ¹⁴C in air samples from aircraft requires detailed dispersion modeling of surface emissions into a highly dynamic atmosphere. Conversely, interpretation of monthly integrated air samples from tall towers requires the inclusion of stratospheric sources and re-emergence of old ¹⁴C signals after longer turn-over in the oceans and biosphere. In a recent publication (Bozhinova et al., 2013), we showed that the interpretation of growing season integrated plant samples additionally requires simulation of location and weather dependent photosynthetic uptake and plant development patterns. A successful ¹⁴C monitoring strategy will thus depend strongly on our ability to capture these diverse processes on diverse scales.

ff – fossil fuels, p – photosynthetic uptake, r – ecosystem respiration, o – ocean, n – nuclear and s – stratospheric.

$$\text{CO}_{2\text{obs}} = \text{CO}_{2\text{bg}} + \text{CO}_{2\text{ff}} + \text{CO}_{2\text{p}} + \text{CO}_{2\text{r}} + \text{CO}_{2\text{o}} \quad (1)$$

$$\Delta_{\text{obs}}\text{CO}_{2\text{obs}} = \Delta_{\text{bg}}\text{CO}_{2\text{bg}} + \Delta_{\text{ff}}\text{CO}_{2\text{ff}} + \Delta_{\text{p}}\text{CO}_{2\text{p}} + \Delta_{\text{r}}\text{CO}_{2\text{r}} + \Delta_{\text{o}}\text{CO}_{2\text{o}} + \Delta_{\text{n}}^{14}\text{CO}_{2\text{n}} + \Delta_{\text{s}}\text{CO}_{2\text{s}} \quad (2)$$

Several of the terms in both equations can be omitted or transformed in our study, as described next.

We set $\Delta_{\text{p}} = \Delta_{\text{bg}}$ similar to the approach in Turnbull et al. (2006) as the calculation of $\Delta^{14}\text{CO}_2$ accounts for changes in the signature of the photosynthesized CO_2 flux due to fractionation. The atmosphere-ocean exchange in the northern Atlantic makes the region generally a sink of carbon (Watson et al., 2009), but we assume that its transport to our domain is uniform and captured by the inflow of background air and thus also carries the signature Δ_{bg} . For the ecosystem respiration and ocean exchange the terms Δ_{r} and Δ_{o} can be also written as $\Delta_{\text{bg}} + \Delta_{\text{bio}}^{\text{dis}}$ and $\Delta_{\text{bg}} + \Delta_{\text{ocean}}^{\text{dis}}$, where the disequilibrium terms (Δ^{dis}) describe the difference between the signature of the carbon in the particular reservoir and the current atmospheric background. These differences arise from the past enrichment of the atmosphere with $^{14}\text{CO}_2$ from the atmospheric nuclear bomb tests since the 1960s. In the following decades this enrichment was incorporated into the different carbon reservoirs (Levin and Kromer, 1997; Levin and Heshaimer, 2000) and currently these terms are of dominant importance only in particular regions of the globe. For our domain both terms are of much smaller influence than the dominant effect of the fossil fuels and are consequently omitted (Levin and Karstens, 2007; Hsueh et al., 2007; Palstra et al., 2008; Turnbull et al., 2009b; Naegler and Levin, 2009a, b; Levin et al., 2010). The intrusion of $^{14}\text{CO}_2$ -enriched stratospheric air can be of importance for observations in the upper troposphere or higher, however in our case this term can be considered as part of the background, as the stratospheric $^{14}\text{CO}_2$ is already well mixed by the time it reaches the lower troposphere.

Modeling $\Delta^{14}\text{CO}_2$ for Western Europe

D. Bozhinova et al.

Title Page

Abstract

Introduction

Conclusions

References

Tables

Figures

◀

▶

◀

▶

Back

Close

Full Screen / Esc

Printer-friendly Version

Interactive Discussion



Modeling $\Delta^{14}\text{CO}_2$ for Western Europe

D. Bozhinova et al.

Title Page

Abstract

Introduction

Conclusions

References

Tables

Figures

◀

▶

◀

▶

Back

Close

Full Screen / Esc

Printer-friendly Version

Interactive Discussion



Most studies neglect the effects of anthropogenic nuclear production of $^{14}\text{CO}_2$ on the atmospheric $\Delta^{14}\text{CO}_2$ since on the global scale this production averages to the smallest contribution, compared to the other terms (Turnbull et al., 2009a). However, Graven and Gruber (2011) showed that on a regional scale for a domain with a dense nuclear power plant network its influence can not be neglected. They estimated the potential bias in the recalculation of fossil fuel CO_2 due to nuclear power plant production is on average between 0.5 and 1 ppm for Europe, but the horizontal resolution of their transport model ($1.8^\circ \times 1.8^\circ$) limits the analysis for the regions close to the sources. We note that two of the three existing worldwide Spent Fuel Reprocessing Plants are located in Western Europe (SFRP, in La Hague, France and Sellafield, UK), which generally have higher than average emissions of $^{14}\text{CO}_2$. Particularly the site of La Hague is estimated to be the largest point-source of $^{14}\text{CO}_2$ emissions in the world, in recent years accounting for more than 10% of the global budget of nuclear produced $^{14}\text{CO}_2$ (Graven and Gruber, 2011). The magnitude of this source and its spatial location close to the major fossil fuel emitters in Europe pose a challenge in estimating the uncertainty with which the method of recalculating fossil fuel CO_2 can be applied in the region.

All these considerations allow us to simplify Eqs. (1) and (2) to Eqs. (3) and (4).

$$\text{CO}_{2\text{obs}} = \text{CO}_{2\text{bg}} + \text{CO}_{2\text{ff}} + \text{CO}_{2\text{p}} + \text{CO}_{2\text{r}} \quad (3)$$

$$\Delta_{\text{obs}} \text{CO}_{2\text{obs}} = \Delta_{\text{bg}} (\text{CO}_{2\text{bg}} + \text{CO}_{2\text{p}} + \text{CO}_{2\text{r}}) + \Delta_{\text{ff}} \text{CO}_{2\text{ff}} + \Delta_{\text{n}}^{14} \text{CO}_{2\text{n}} \quad (4)$$

The instantaneous $\Delta^{14}\text{CO}_2$ signature of the atmosphere is calculated using Eq. (4), using the specific signatures for various sources of CO_2 (various Δ terms) as listed below:

1. Fossil fuels are entirely devoid of $^{14}\text{CO}_2$ and their $\Delta_{\text{ff}} = -1000\%$.
2. The nuclear emissions are of pure $^{14}\text{CO}_2$ and in this formulation Δ_{n} is the $\Delta^{14}\text{CO}_2$ signature that a pure $^{14}\text{CO}_2$ sample would have. We calculate it using the activity

of pure $^{14}\text{CO}_2$ sample in the formulation of $\Delta^{14}\text{CO}_2$ as follows:

$$A_s = \lambda \cdot N_a / m_{14\text{C}} \quad (5)$$

where $N_a = 6.022 \times 10^{23} \text{ mol}^{-1}$ is the Avogadro constant, $\lambda = 3.8332 \times 10^{-12} \text{ Bq}$ is the decay rate of ^{14}C and $m_{14\text{C}} = 14.0 \text{ g mol}^{-1}$ is the molar mass of the isotope. In a sample of a pure $^{14}\text{CO}_2$ there is no fractionation and the calculation of $\Delta^{14}\text{CO}_2$ (Stuiver and Polach, 1977; Mook and van der Plicht, 1999) can be simplified to the ratio between the activity of the sample and activity of the referenced standard $A_{\text{ABS}} = 0.226 \text{ Bq g C}^{-1}$ (Mook and van der Plicht, 1999):

$$\Delta_n = A_s / A_{\text{ABS}} \cdot 1000 [\text{‰}] \quad (6)$$

The resulting $\Delta_n \approx 0.7 \times 10^{15} [\text{‰}]$ is much higher than any of the other Δ signatures, but this is balanced by the concentrations of the $^{14}\text{CO}_2$, which are only a very small fraction ($\sim 10^{-12}$) of the observed CO_2 concentrations.

3. Finally, we use Δ_{bg} from monthly observed $\Delta^{14}\text{CO}_2$ at the high alpine station Jungfraujoch (3580 m a.s.l., Switzerland) (Levin et al., 2010), which is considered representative for European $\Delta^{14}\text{CO}_2$ background. These are shown in red on Fig. 2b.

The transport and resulting spatiotemporal gradients in total CO_2 and $^{14}\text{CO}_2$ over Europe are simulated with WRF-CHEM model, described next.

2.2 WRF-CHEM

For our simulation with WRF-Chem (version 3.2.1) (Skamarock et al., 2008) we use meteorological fields from the NCEP FNL Operational Model Global Tropospheric Analyses (NCEP, US National Centers for Environmental Prediction, 2013) for lateral meteorological boundary conditions, which are updated every 6 h. We use three domains

Modeling $\Delta^{14}\text{CO}_2$ for Western Europe

D. Bozhinova et al.

[Title Page](#)[Abstract](#)[Introduction](#)[Conclusions](#)[References](#)[Tables](#)[Figures](#)[◀](#)[▶](#)[◀](#)[▶](#)[Back](#)[Close](#)[Full Screen / Esc](#)[Printer-friendly Version](#)[Interactive Discussion](#)

with horizontal resolution of 36 km, 12 km and 4 km and respectively 60×62 , 109×100 and 91×109 grid points, centered over Western Europe and the Netherlands. Our vertical resolution includes 27 pressure levels, 18 of which are in the lower 2 km of the troposphere, and the time step used is 180 s in the outer domain. Important physics schemes used are the MYNN2.5 boundary layer scheme (Nakanishi and Niino, 2006), RRTM long wave radiation (Mlawer et al., 1997), and Dudhia shortwave radiation (Dudhia, 1989). We use the Unified Noah LSM (Ek et al., 2003) as our surface physics scheme and additionally use time-varying surface conditions, which we update every 6 h.

We use separate passive tracers for the different CO_2 terms in Eq. (4). We prescribe our initial and lateral boundary conditions for the background CO_2 , while the biospheric uptake, respiration, fossil fuel CO_2 and nuclear $^{14}\text{CO}_2$ are implemented with surface fluxes only, which are prescribed and provided to the model every hour. This is partially a consequence of our interest in the recent influence of the biosphere and anthropogenic emissions and once these CO_2 signals leave our outer domain they will not re-enter it again. For this reason we will avoid using direct results from the outer domain, and instead use only the nested domains, where boundary conditions for all tracers are provided through their respective mother domain.

The background ($\text{CO}_{2\text{bg}}$) initial and boundary conditions are implemented using 3-D mole fraction output from Carbon Tracker (Peters et al., 2010) for 2008 at $1^\circ \times 1^\circ$ resolution and interpolated vertically from 34 to 27 levels using the pressure fields. The CO_2 lateral boundary conditions are added to the standard meteorological boundary conditions and also updated every 6 h.

Our biospheric fluxes ($\text{CO}_{2\text{r}}$ and $\text{CO}_{2\text{p}}$) are generated using the SiBCASA model (Schaefer et al., 2008), which used meteo fields from the European Centre for Medium-Range Weather Forecasts (ECMWF). It provides us with monthly averaged gross photosynthetic production (GPP) and terrestrial ecosystem respiration (TER) at $1^\circ \times 1^\circ$ resolution. Due to the coarse resolution of the SiBCASA model, we find land-use categories in the higher resolution map of WRF that are not in the natural land-use map of

Modeling $\Delta^{14}\text{CO}_2$ for Western Europe

D. Bozhinova et al.

Title Page

Abstract

Introduction

Conclusions

References

Tables

Figures

I◀

▶I

◀

▶

Back

Close

Full Screen / Esc

Printer-friendly Version

Interactive Discussion



SiBCASA. To address this issue, we ran 9 simulations with SiBCASA prescribing a single vegetation category, alternating through all the vegetation categories to produce biospheric fluxes for the different land-use categories within the resolution of WRF. For temporal interpolation of the monthly fluxes, we scale the GPP and TER with the instantaneous WRF meteorological variables (temperature at 2 m and shortwave solar radiation) following the method described in Olsen and Randerson (2004). We first scale the SiBCASA output using the monthly mean averaged radiation (for GPP) and a Q_{10} relation towards the monthly averaged temperature (for TER). These scaled down fluxes are then prescribed in the WRF model on an hourly basis and multiplied with the WRF calculated shortwave radiation and Q_{10} at every time step.

Anthropogenic (fossil fuel) CO_2 emissions ($\text{CO}_{2\text{ff}}$) are provided by the CarboEurope project (IER, Stuttgart, Pregger et al., 2007) at 5 (geographical) minutes horizontal resolution over Europe in the form of annual emission at the location and temporal profiles to add variability during different months, weekdays and hours during the day. These are then aggregated to every WRF domain horizontal resolution and updated every hour for the duration of our simulation. The emissions are introduced only at the lowest (surface) level of the model.

Anthropogenic (nuclear) $^{14}\text{CO}_2$ emissions ($^{14}\text{CO}_{2\text{n}}$) are obtained by applying the method described in Graven and Gruber (2011) for the year of 2008. We used information from the International Atomic Energy Agency Power Reactor Information System (IAEA PRIS, available online at <http://www.iaea.org/pris>) for the energy production of the nuclear reactors in our domain and reported $^{14}\text{CO}_2$ discharges for the spent fuel reprocessing sites (van der Stricht and Janssens, 2010). These were scaled down directly from annual to hourly emissions, assuming that these emissions are continuous and constant during the year. We will further comment on these assumptions in our Discussion (Sect. 4).

2.3 Integrated $\Delta^{14}\text{CO}_2$ air and plant samples

Integrated $\Delta^{14}\text{CO}_2$ samples ($\Delta_{\text{absorption}}$), where the sampling rate is usually constant (e.g. in various CO_2 absorption setups), are represented with the concentration-weighted time-average $\Delta^{14}\text{CO}_2$ signature for the period and height of sampling, as seen in Eq. (7):

$$\Delta_{\text{absorption}} = \sum_t \Delta_{\text{obs}}^t \frac{\text{CO}_{2\text{obs}}^t}{\sum_t \text{CO}_{2\text{obs}}^t} \quad (7)$$

Plant samples (Δ_{plant}) integrate the atmospheric $\Delta^{14}\text{CO}_2$ signature with CO_2 assimilation rate which varies depending on various meteorological and phenological factors. Photosynthetic uptake and the allocation of the assimilated CO_2 in the different plant parts strongly depend on the weather conditions and plant development. To simulate such samples we use WRF meteorological fields in the crop growth model SUCROS2 (van Laar et al., 1997) and use the modeled daily growth increment as a weighting function (averaging kernel) on the daytime atmospheric $\Delta^{14}\text{CO}_2$ signatures (Bozhinova et al., 2013). For each location we use the same sowing date and the model simulates the crop development until it reaches flowering, when we calculate Δ_{plant} . More explicitly these integrated sample signatures are calculated as:

$$\Delta_{\text{plant}} = \sum_t \Delta_{\text{obs}}^t \frac{X_t}{\sum_t X_t}, \quad (8)$$

where X_t is the growth increment at time t , which in the case of SUCROS2 simulation is the dry matter weight increment at day t .

Title Page

Abstract

Introduction

Conclusions

References

Tables

Figures

◀

▶

◀

▶

Back

Close

Full Screen / Esc

Printer-friendly Version

Interactive Discussion



derived fossil fuel CO₂ estimates show good agreement with our model results in that period and this could indicate a possible issue with the $\Delta^{14}\text{CO}_2$ observations by themselves. Note that even though station Lutjewad is distant to nuclear emission sources, the signal from nuclear activity (shown in the last pannel) can be occasionally of the same order of magnitude as the fossil fuel signal. This shows how important it is to evaluate the nuclear influence at every measurement site, as it will contribute to the uncertainty in the recalculation of fossil fuel CO₂.

3.2 Fossil fuel vs. nuclear emissions influence on $\Delta^{14}\text{CO}_2$

The lowest $\Delta^{14}\text{CO}_2$ values in the domain are modeled in the regions with high fossil fuel emission in west Germany (the Ruhrgebiet), and the highest $\Delta^{14}\text{CO}_2$ is near the large emitting sites in Western France and UK. This pattern can be clearly seen in Fig. 4a–c where results for average situation in the lower 1200 m of the atmosphere over the 6 months are shown. Note that the nuclear enrichment reaches much higher amplitude than the opposite effect by the fossil CO₂, but its influence on the atmospheric $\Delta^{14}\text{CO}_2$ is usually on the local scale around the average nuclear power plant reactors. The influence is more pronounced in the west part of our domain, where it captures the influence from the SFRP in La Hague (France) and several newer generation nuclear reactors in the UK. Even then, the influence of the nuclear enrichment averaged over 6 months is mostly about 1 to 6‰ in areas that are not in direct vicinity of the sources. As a comparison, the fossil fuel influence in our domain on the same temporal and spatial scale is mostly between –3 and –15‰ outside the very polluted area of the Ruhrgebiet, Germany.

As the nuclear enrichment will (partially) mask the effect of fossil fuel CO₂ on the atmospheric $\Delta^{14}\text{CO}_2$, we show in Fig. 4d the average 6 month ratio of the influences due to nuclear and fossil fuel sources in our domain. Again, in most of the east and central parts of our domain the nuclear influence is less than 10 % the fossil fuel influence. This differs from the west part of our domain, where the ratio varies between 3 times smaller

Modeling $\Delta^{14}\text{CO}_2$ for Western Europe

D. Bozhinova et al.

Title Page

Abstract

Introduction

Conclusions

References

Tables

Figures

◀

▶

◀

▶

Back

Close

Full Screen / Esc

Printer-friendly Version

Interactive Discussion



Modeling $\Delta^{14}\text{CO}_2$ for Western Europe

D. Bozhinova et al.

Title Page

Abstract

Introduction

Conclusions

References

Tables

Figures

◀

▶

◀

▶

Back

Close

Full Screen / Esc

Printer-friendly Version

Interactive Discussion



to about the same magnitude as the fossil fuel contribution and even to a more than 5 times larger influence in the area around the nuclear sources. These findings are consistent with Graven and Gruber (2011) and the improvement in the horizontal resolution of the transport model results in a much larger nuclear enrichment in the grid box containing a nuclear source. The magnitude and size of the influenced area are highly variable and strongly dependent on the atmospheric transport. As a result, in months with dominant easterly winds the nuclear enrichment has a minimum effect in our domain, as most of the nuclear emissions are transported towards the Atlantic ocean and out of our area of interest. However, in months with dominant westerly winds, which is the more often the observed case, the nuclear $^{14}\text{CO}_2$ spreads widely over the domain.

For sites located in Northern and Central France, Southern Germany and the UK the nuclear enrichment means that corrections are needed that account for the nuclear influence in the observed $\Delta^{14}\text{CO}_2$ before estimating the fossil fuel influence. As an illustration, we show the influence of the different anthropogenic emissions for three locations with different characteristics in our domain, in Fig. 5: Cambridge (UK), Cabauw (the Netherlands) and Kosetice (Czech Republic). The locations were chosen to be in rural or agricultural areas, without large local CO_2 emissions. As seen in Fig. 5, the west part of our domain (represented by Cambridge) has an equal influence from fossil fuel and nuclear emissions; the center (represented by Cabauw) does see some events with relatively high nuclear emissions influence, but is defined mostly by the very high fossil fuel emissions in this region, which are on average about 3 times higher than in Cambridge. In the east (represented by Kosetice) there is no significant signal of nuclear emissions, but the fossil fuel emissions influence is also considerably lower.

3.3 $\Delta^{14}\text{CO}_2$ plant vs. atmospheric samples

In our previous work (Bozhinova et al., 2013) we described a method to model the $\Delta^{14}\text{CO}_2$ in plant samples as the first step in quantifying the differences between such samples and integrated atmospheric samples. Here we build on this work by calculating the plant signature resulting from uptake of spatially and temporally variable atmo-

spheric $\Delta^{14}\text{CO}_2$. The results for modeled samples from maize leaves at flowering, are shown in Fig. 6. Clearly, spatial gradients in $\Delta^{14}\text{CO}_2$ in plants are sizeable compared to the measurement precision of approximately 2%. The regions with high influence from anthropogenic emissions from Fig. 4, namely the Ruhrgebiet in West Germany and the Benelux are also visible in the modeled plant signature, and so are some hotspots around larger european cities, like Frankfurt, Paris, London and others. It is important to point out that in addition to fossil fuel and nuclear gradients, plants develop at different rates in different parts of the domain, and even the different parts of a plant (roots, stems, leaves, fruits) grow during different time periods.

The plant-sampled $\Delta^{14}\text{CO}_2$ includes the effect of the covariance between the atmospheric $\Delta^{14}\text{CO}_2$ variability and the variability in the assimilation of CO_2 in the plant during growth, which is absent in traditional integrated samples where the absorption of CO_2 is based on constant flow rate through an alkaline solution and thus only varies with the CO_2 concentration present in the flow (Hsueh et al., 2007). In Fig. 7 we show this effect of the plant growth on the resulting plant $\Delta^{14}\text{CO}_2$ signature. We should stress, that this is the magnitude of the error one should expect if the plant sampled $\Delta^{14}\text{CO}_2$ is assumed equal to the atmospheric mean $\Delta^{14}\text{CO}_2$ for the growing period of the plant. For many parts of Europe in our simulated period this error is approaching the measurement precision of the $\Delta^{14}\text{CO}_2$ analysis (of approximately $\pm 2\%$). In the region located between the areas with high fossil fuel and large nuclear emitters, however, the magnitude of the error can be several times larger. This is likely due to the absorption of some very high signature values on a few specific days when the wind direction is directly from the nuclear source. Actual plant samples, taken during different period than the one investigated here (namely 2010–2012), will be used to further investigate these signatures in a follow-up publication.

Modeling $\Delta^{14}\text{CO}_2$ for Western Europe

D. Bozhinova et al.

Title Page

Abstract

Introduction

Conclusions

References

Tables

Figures

◀

▶

◀

▶

Back

Close

Full Screen / Esc

Printer-friendly Version

Interactive Discussion



3.4 Direct estimation of the fossil fuel CO₂ emissions

As an alternative to modeling of the ¹⁴CO₂ budget as presented here, we searched for a possible direct relationship between the prescribed regional emissions and the resulting $\Delta^{14}\text{CO}_2$ signal that would be observed in air samples or plants. While the entire emission map of Europe might be difficult to verify, most of the fossil fuel CO₂ emissions are produced at only a number of sites. This provides an opportunity where only the chosen sites are object of a sampling campaign or study, but these can still provide a better estimate for the highest emitting regions in Europe. As an illustration, 10% of all emissions in our domain are emitted from only 30 grid cells and more than half of these are already located in densely populated cities or urban conglomerations. We focused our following analysis on the top 25 populated cities and top 30 emitting grids in our domain with 12 km horizontal resolution.

We looked into the relationship between the $\Delta^{14}\text{CO}_2$ signatures modeled at the surface for each of the locations and the emissions we prescribe in our model. Regarding the $\Delta^{14}\text{CO}_2$ signatures we used for this analysis, we compared the set of modeled daytime integrated samples, 24 h integrated samples, and samples modeled for maize leaves. Regarding the fossil fuel emissions, we compared each set of modeled $\Delta^{14}\text{CO}_2$ samples with its according prescribed emissions at the exact grid cell where the $\Delta^{14}\text{CO}_2$ sample was modeled, and additionally to the prescribed emissions, but averaged over a 5 × 5 grid around it (area-averaged). In all cases, the comparison for the emissions prescribed at the exact location showed some, but quite low correlation, which was considerably higher when comparing to the area-averaged emissions.

After constructing the linear fit to each of these relationships, we used it to recalculate the fossil fuel emissions we would estimate if using only the linear relation and the simulated $\Delta^{14}\text{CO}_2$ at each location, and evaluated the RMSD between the prescribed emissions and those estimated afterwards. The best relation we found (i.e., the one that gave the smallest RMSD of the linear fit) was when considering the $\Delta^{14}\text{CO}_2$ signatures for the top 25 cities modeled in maize leaves and compared to the area-averaged emis-

Modeling $\Delta^{14}\text{CO}_2$ for Western Europe

D. Bozhinova et al.

[Title Page](#)[Abstract](#)[Introduction](#)[Conclusions](#)[References](#)[Tables](#)[Figures](#)[◀](#)[▶](#)[◀](#)[▶](#)[Back](#)[Close](#)[Full Screen / Esc](#)[Printer-friendly Version](#)[Interactive Discussion](#)

Modeling $\Delta^{14}\text{CO}_2$ for Western Europe

D. Bozhinova et al.

Title Page

Abstract

Introduction

Conclusions

References

Tables

Figures

◀

▶

◀

▶

Back

Close

Full Screen / Esc

Printer-friendly Version

Interactive Discussion



the method of using $\Delta^{14}\text{CO}_2$ to calculate the fossil fuel CO_2 addition to the regional atmosphere. The strongest gradients of $\Delta^{14}\text{CO}_2$ in Western Europe are found in the relatively polluted region in Western Germany and the Netherlands due to the high population density and large industry sector there, and hence high CO_2 emissions. More detailed $^{14}\text{CO}_2$ observations in this region can possibly prove useful in lowering the uncertainty of the regional fossil fuel emission estimates as also investigated for California by Riley et al. (2008). Furthermore, the high fossil-to-nuclear ratio ensures that uncertainties arising from nuclear emissions will be at their minimum.

This result relies partly on the underlying emission maps for the anthropogenic (fossil fuel) CO_2 and (nuclear) $^{14}\text{CO}_2$ emissions. We should consider various factors that are uncertain or unknown at this point for these emissions (Peylin et al., 2011; Graven and Gruber, 2011) – such as temporal characters, vertical resolution and even small irregularities in the spatial allocation of the emission sources. All our anthropogenic emissions are located in the lowest (surface) layer of our model, however the vertical discretisation is possibly up for improvement. Most of the industrial emission stacks are located at 100 to 300 m height and applying this information, where available, in our input data will likely result in the emissions being transported further away faster and result in less local enrichment. For the fossil fuel CO_2 emissions we apply temporal profiles that disaggregate monthly, weekly and diurnal signals from the provided annual emissions. For the nuclear emissions such profiles are unknown and information on their temporal heterogeneity is not publically available. In this study we consider them as continuous and constant throughout the year. This is a relatively safe assumption for the emissions from nuclear power plants as their $^{14}\text{CO}_2$ is a by-product of the normal operation of the reactor. This might not be the case for reprocessing sites, where the emissions will depend also on the type and amount of fuel being reprocessed. Additionally, there is uncertainty if these emissions are released continuously or in few timed or instantaneous big venting events, and the venting procedures are likely reactor-type dependent.

Modeling $\Delta^{14}\text{CO}_2$ for Western Europe

D. Bozhinova et al.

Title Page

Abstract

Introduction

Conclusions

References

Tables

Figures

◀

▶

◀

▶

Back

Close

Full Screen / Esc

Printer-friendly Version

Interactive Discussion



When using flask samples for $^{14}\text{CO}_2$ measurement nuclear enrichment can relatively easily be recognized. However, in integrated air and plant samples this signal will be averaged over the total sampling period. These latter samples will record the enrichment in $\Delta^{14}\text{CO}_2$, but depending on the weather variability, local fossil fuel CO_2 addition and the proximity to the nuclear sources, these signals can be within the measurement precision (of approximately $\pm 2\%$). Integrated samples are thus likely of too low time-resolution to attribute nuclear emissions, and areas where this influence is high would profit from flask sampling of $\Delta^{14}\text{CO}_2$ in addition to integrated sampling. If the nuclear emissions occur in less frequent but larger events as speculated above, the integrated samples are likely to be influenced less, and the flask samples are less likely to capture such events. Overall, we deem a better characterization of the temporal structure of the nuclear emissions a prerequisite for any $^{14}\text{CO}_2$ -based monitoring effort in Europe.

We should note that our study is also subject to known uncertainties in atmospheric transport of current mesoscale models. An inaccurate simulation of wind speed and direction (Lin and Gerbig, 2005; Gerbig et al., 2008; Ahmadov et al., 2009) or boundary layer height development (Vilà-Guerau de Arellano et al., 2004; Steeneveld et al., 2008; Pino et al., 2012) will all affect the transport of emission plumes and resulting mole fractions. Resolving more meso-scale circulations, and improved representation of topography can be particularly advantageous, as they can cause large gradients in CO_2 (de Wekker et al., 2005; van der Molen and Dolman, 2007). While WRF-Chem is used for a variety of atmospheric transport studies (among others: Tie et al., 2009; de Foy et al., 2011; Lee et al., 2011; Stuefer et al., 2013), more general air quality studies have shown that an ensemble model can forecast air pollution situations more accurately than a single separate model (Galmarini et al., 2004, 2013). While in our research we focused on the passive transport of CO_2 and $^{14}\text{CO}_2$, other chemical species are already available in the core of WRF-Chem. Another step further could be the addition of such chemically active tracers (e.g. CO , NO_x , and many others) that are regularly measured with regards to air pollution and health safety and connected with anthropogenic emissions that are the ultimate interest of our study. Including ^{222}Rn as

Modeling $\Delta^{14}\text{CO}_2$ for
Western Europe

D. Bozhinova et al.

Title Page

Abstract

Introduction

Conclusions

References

Tables

Figures

◀

▶

◀

▶

Back

Close

Full Screen / Esc

Printer-friendly Version

Interactive Discussion



additional tracer can be very beneficial for lowering the uncertainty associated with the vertical mixing in the model and provide correction factors to be applied to the other passive tracers, as shown in van der Laan et al. (2010), Vogel et al. (2013).

Considering future uses of $\Delta^{14}\text{CO}_2$ observations as additional constraint on the carbon cycle by the atmospheric modeling community, we should note that atmospheric inversions can use only afternoon observational data. In that case, plant-sampled $\Delta^{14}\text{CO}_2$ observations may provide a better representation of the afternoon atmospheric $\Delta^{14}\text{CO}_2$ signals than conventional integrated samples that also absorb CO_2 during the night.

We explored the possibility that a relatively simple relationship can be used to calculate the emissions directly from $\Delta^{14}\text{CO}_2$ observations. While the method seems promising, its inability to capture bigger part of the variability in the modeled $\Delta^{14}\text{CO}_2$ signals condemns it to high inherent uncertainty for the reconstructed emissions. While a portion of this uncertainty can be lowered with a better fitting relationship, another is a direct consequence by the $\Delta^{14}\text{CO}_2$ measurement precision and will provide a lower limit to the reconstructed emissions.

Our results suggest that a combination of the available sampling methods should be used when planning a $^{14}\text{CO}_2$ observational network for the purpose of fossil fuel emissions investigations. Integrated air and plant samples alone can provide a longer period observations at a lower cost, but this feature makes them less useful for evaluation of large nuclear influences in shorter periods. Flask samples are much better suited for this exact task, however their continuous analysis is too costly in the long run. A possible compromise could be obtaining flask samples for a limited period alongside integrated samples for new sampling locations. This would already provide information about the possible nuclear enrichment and the wind directions from which it usually occurs. Additionally, while integrated air samples are the current standard for quasi-continuous observations of $^{14}\text{CO}_2$ and the uncertainties in their CO_2 assimilation are lower, plant samples can be obtained at a much higher spatial resolution without additional infrastructure investment. Their use is constrained to the sunlit part of the day,

and time and locations where the chosen crop grows, but that should not limit their use to help us verify spatial patterns and gradients.

5 Conclusions

In this work, we demonstrated the ability of our modeling framework to simulate the atmospheric transport of CO_2 and consequently the atmospheric $\Delta^{14}\text{CO}_2$ signature in integrated air and plant samples in Western Europe. Based on our investigation and results we reach the following conclusions.

1. Simulated spatial gradients of $\Delta^{14}\text{CO}_2$ are of measurable size and the 6 month average $\text{CO}_{2\text{ff}}$ concentrations in the lower 1 km of the atmosphere across Western Europe are between 1 to 18 ppm.
2. Enrichment by $^{14}\text{CO}_2$ from nuclear sources can, at least partly, mask the Suess effect nearby the sources of nuclear emissions, particularly in large parts of UK and North-Western France. This is consistent with previous studies (Graven and Gruber, 2011) and we show that in these regions the strength of the nuclear influence can be comparable and even larger than the influence from fossil fuel emissions.
3. The simulated plant $\Delta^{14}\text{CO}_2$ signatures show spatial gradients consistent with the simulated atmospheric gradients and many emission hotspots are clearly visible in the modeled plant samples. Plant growth variability induces differences between the simulated plant and the atmospheric mean of magnitude which are mostly within the measurement precision of $\pm 2\%$, but of up to $\pm 7\%$ in some areas.
4. Integrated $\Delta^{14}\text{CO}_2$ from areas outside the immediate enrichment area of nuclear emission sources are not sensitive to occasional advection of enriched air due to their long absorption period. However, to properly account for the nuclear enrich-

Modeling $\Delta^{14}\text{CO}_2$ for Western Europe

D. Bozhinova et al.

Title Page

Abstract

Introduction

Conclusions

References

Tables

Figures

◀

▶

◀

▶

Back

Close

Full Screen / Esc

Printer-friendly Version

Interactive Discussion



Modeling $\Delta^{14}\text{CO}_2$ for
Western Europe

D. Bozhinova et al.

Title Page

Abstract

Introduction

Conclusions

References

Tables

Figures

◀

▶

◀

▶

Back

Close

Full Screen / Esc

Printer-friendly Version

Interactive Discussion



ance. Part 1: Fossil fuel emissions, *Glob. Change Biol.*, 16, 1395–1408, doi:10.1111/j.1365-2486.2009.02098.x, 2010. 30613

de Foy, B., Burton, S. P., Ferrare, R. A., Hostetler, C. A., Hair, J. W., Wiedinmyer, C., and Molina, L. T.: Aerosol plume transport and transformation in high spectral resolution lidar measurements and WRF-Flexpart simulations during the MILAGRO Field Campaign, *Atmos. Chem. Phys.*, 11, 3543–3563, doi:10.5194/acp-11-3543-2011, 2011. 30631

de Wekker, S. F. J., Steyn, D. G., Fast, J. D., Rotach, M. W., and Zhong, S.: The performance of RAMS in representing the convective boundary layer structure in a very steep valley, *Environ. Fluid Mech.*, 5, 35–62, doi:10.1007/s10652-005-8396-y, 2005. 30631

Djuricin, S., Pataki, D. E., and Xu, X.: A comparison of tracer methods for quantifying CO_2 sources in an urban region, *J. Geophys. Res.-Atmos.*, 115, D11303, doi:10.1029/2009JD012236, 2010. 30613

Dudhia, J.: Numerical study of convection observed during the Winter Monsoon Experiment using a mesoscale two-dimensional model, *J. Atmos. Sci.*, 46, 3077–3107, 1989. 30620

Ek, M., Mitchell, K., Lin, Y., Rogers, E., Grunmann, P., Koren, V., Gayno, G., and Tarpley, J.: Implementation of NOAA land surface model advances in the National Centers for Environmental Prediction operational mesoscale Eta model, *J. Geophys. Res.-Atmos.*, 108, 8851, doi:10.1029/2002JD003296, 2003. 30620

Francey, R., Trudinger, C., van der Schoot, M., Law, R., Krummel, P., Langenfelds, R., Steele, L. P., Allison, C., Stavert, A., Andres, R., and Rodenbeck, C.: Atmospheric verification of anthropogenic CO_2 emission trends, *Nature Clim. Change*, 3, 520–524, doi:10.1038/nclimate1817, 2013. 30613

Friedlingstein, P., Houghton, R., Marland, G., Hackler, J., Boden, T., Conway, T., Canadell, J., Raupach, M., Ciais, P., and Quéré, C. L.: Update on CO_2 emissions, *Nat. Geosci.*, 3, 811–812, 2010. 30612

Galmarini, S., Bianconi, R., Addis, R., Andronopoulos, S., Astrup, P., Bartzis, J., Bellasio, R., Buckley, R., Champion, H., Chino, M., D'Amours, R., Davakis, E., Eleveld, H., Glaab, H., Manning, A., Mikkelsen, T., Pechinger, U., Polreich, E., Prodanova, M., Slaper, H., Syrakov, D., Terada, H., and Auwera, L. V. D.: Ensemble dispersion forecasting – Part II: Application and evaluation, *Atmos. Environ.*, 38, 4619–4632, 2004. 30631

Galmarini, S., Kioutsioukis, I., and Solazzo, E.: *E pluribus unum**: ensemble air quality predictions, *Atmos. Chem. Phys.*, 13, 7153–7182, doi:10.5194/acp-13-7153-2013, 2013. 30631

Modeling $\Delta^{14}\text{CO}_2$ for
Western Europe

D. Bozhinova et al.

Title Page

Abstract

Introduction

Conclusions

References

Tables

Figures

◀

▶

◀

▶

Back

Close

Full Screen / Esc

Printer-friendly Version

Interactive Discussion



Gerbig, C., Körner, S., and Lin, J. C.: Vertical mixing in atmospheric tracer transport models: error characterization and propagation, *Atmos. Chem. Phys.*, 8, 591–602, doi:10.5194/acp-8-591-2008, 2008. 30631

Godwin, H.: Half-life of radiocarbon, *Nature*, 195, p. 984, 1962. 30614

5 Graven, H. D. and Gruber, N.: Continental-scale enrichment of atmospheric $^{14}\text{CO}_2$ from the nuclear power industry: potential impact on the estimation of fossil fuel-derived CO_2 , *Atmos. Chem. Phys.*, 11, 12339–12349, doi:10.5194/acp-11-12339-2011, 2011. 30616, 30618, 30621, 30626, 30630, 30633

10 Graven, H. D., Guilderson, T. P., and Keeling, R. F.: Observations of radiocarbon in CO_2 at La Jolla, California, USA 1992–2007: Analysis of the long-term trend, *J. Geophys. Res.-Atmos.*, 117, D02302, doi:10.1029/2011JD016533, 2012a. 30614

Graven, H. D., Guilderson, T. P., and Keeling, R. F.: Observations of radiocarbon in CO_2 at seven global sampling sites in the Scripps flask network: Analysis of spatial gradients and seasonal cycles, *J. Geophys. Res.-Atmos.*, 117, D02303, doi:10.1029/2011JD016535, , 2012b. 30614

15 Gurney, K., Mendoza, D., Zhou, Y., Fischer, M., Miller, C., Geethakumar, S., and Can, S. D.: High resolution fossil fuel combustion CO_2 emission fluxes for the United States, *Environ. Sci. Technol.*, 43, 5535–5541, 2009. 30613

20 Hsueh, D. Y., Krakauer, N. Y., Randerson, J. T., Xu, X., Trumbore, S. E., and Southon, J. R.: Regional patterns of radiocarbon and fossil fuel-derived CO_2 in surface air across North America, *Geophys. Res. Lett.*, 34, L02816, doi:10.1029/2006GL027032, 2007. 30614, 30615, 30616, 30617, 30627

Koffi, E. N., Rayner, P. J., Scholze, M., Chevallier, F., and Kaminski, T.: Quantifying the constraint of biospheric process parameters by CO_2 concentration and flux measurement networks through a carbon cycle data assimilation system, *Atmos. Chem. Phys.*, 13, 10555–10572, doi:10.5194/acp-13-10555-2013, 2013. 30613

25 Kuc, T., Rozanski, K., Zimnoch, M., Necki, J., and Korus, A.: Anthropogenic emissions of CO_2 and CH_4 in an urban environment, *Appl. Energ.*, 75, 193–203, 2003. 30613

30 Lee, S.-H., Kim, S.-W., Trainer, M., Frost, G. J., McKeen, S. A., Cooper, O. R., Flocke, F., Holloway, J. S., Neuman, J. A., Ryerson, T., Senff, C. J., Swanson, A. L., and Thompson, A. M.: Modeling ozone plumes observed downwind of New York City over the North Atlantic Ocean during the ICARTT field campaign, *Atmos. Chem. Phys.*, 11, 7375–7397, doi:10.5194/acp-11-7375-2011, 2011. 30631

Modeling $\Delta^{14}\text{CO}_2$ for Western Europe

D. Bozhinova et al.

Title Page

Abstract

Introduction

Conclusions

References

Tables

Figures

◀

▶

◀

▶

Back

Close

Full Screen / Esc

Printer-friendly Version

Interactive Discussion



Levin, I. and Hesshaimer, V.: Radiocarbon – a unique tracer of global carbon cycle dynamics, *Radiocarbon*, 42, 69–80, available at: <https://journals.uair.arizona.edu/index.php/radiocarbon/article/view/3855/3280>, 2000. 30614, 30617

Levin, I. and Karstens, U.: Inferring high-resolution fossil fuel CO_2 records at continental sites from combined $^{14}\text{CO}_2$ and CO observations, *Tellus B*, 59, 245–250, 2007. 30613, 30615, 30617

Levin, I. and Kromer, B.: Twenty years of atmospheric $^{14}\text{CO}_2$ observations at Schauinsland station, Germany, *Radiocarbon*, 39, 205–218, 1997. 30617

Levin, I. and Rödenbeck, C.: Can the envisaged reductions of fossil fuel CO_2 emissions be detected by atmospheric observations?, *Naturwissenschaften*, 95, 203–208, 2008. 30613

Levin, I., Munnich, K., and Weiss, W.: The effect of anthropogenic CO_2 and ^{14}C sources on the distribution of ^{14}C in the atmosphere, *Radiocarbon*, 22, 379–391, 1980. 30614

Levin, I., Schuchard, J., Kromer, B., and Munnich, K. O.: The continental European Suess effect, *Radiocarbon*, 31, 431–440, 1989. 30614

Levin, I., Kromer, B., Schmidt, M., and Sartorius, H.: A novel approach for independent budgeting of fossil fuel CO_2 over Europe by $^{14}\text{CO}_2$ observations, *Geophys. Res. Lett.*, 30, 2194, doi:10.1029/2003GL018477, 2003. 30613, 30616

Levin, I., Hammer, S., Kromer, B., and Meinhardt, F.: Radiocarbon observations in atmospheric CO_2 : determining fossil fuel CO_2 over Europe using Jungfraujoch observations as background, *Sci. Total. Environ.*, 391, 211–216, 2008. 30613

Levin, I., Naegler, T., Kromer, B., Diehl, M., Francey, R. J., Gomez-Pelaez, A. J., Steele, L. P., Wagenbach, D., Weller, R., and Worthy, D. E.: Observations and modelling of the global distribution and long-term trend of atmospheric $^{14}\text{CO}_2$, *Tellus B*, 62, 26–46, doi:10.1111/j.1600-0889.2009.00446.x, 2010. 30614, 30617, 30619

Levin, I., Kromer, B., and Hammer, S.: Atmospheric $\Delta^{14}\text{CO}_2$ trend in Western European background air from 2000 to 2012, *Tellus B*, 65, 20092, doi:10.3402/tellusb.v65i0.20092, 2013. 30624

Libby, W.: Atmospheric helium three and radiocarbon from cosmic radiation, *Phys. Rev.*, 671–672, doi:10.1103/PhysRev.69.671.2, 1946. 30614

Lin, J. C. and Gerbig, C.: Accounting for the effect of transport errors on tracer inversions, *Geophys. Res. Lett.*, 32, L01802, doi:10.1029/2004GL021127, 2005. 30631

Lopez, M., Schmidt, M., Delmotte, M., Colomb, A., Gros, V., Janssen, C., Lehman, S. J., Mondelain, D., Perrussel, O., Ramonet, M., Xueref-Remy, I., and Bousquet, P.: CO, NO_x and 30637

Modeling $\Delta^{14}\text{CO}_2$ for Western Europe

D. Bozhinova et al.

Title Page

Abstract

Introduction

Conclusions

References

Tables

Figures

◀

▶

◀

▶

Back

Close

Full Screen / Esc

Printer-friendly Version

Interactive Discussion



- $^{13}\text{CO}_2$ as tracers for fossil fuel CO_2 : results from a pilot study in Paris during winter 2010, Atmos. Chem. Phys., 13, 7343–7358, doi:10.5194/acp-13-7343-2013, 2013. 30613, 30615
- Marland, G.: Uncertainties in Accounting for CO_2 From Fossil Fuels, J. Ind. Ecol., 12, 136–139, doi:10.1111/j.1530-9290.2008.00014.x, 2008. 30613
- 5 Marland, G. and Rotty, R.: Carbon dioxide emissions from fossil fuels: a procedure for estimation and results for 1950–1982, Tellus B, 36, 232–261, doi:10.1111/j.1600-0889.1984.tb00245.x, 1984. 30613
- McCartney, M. and Baxter, M.: Carbon-14 discharges from the nuclear fuel cycle: 1. Global effects, J. Environm. Radioactiv., 8, 143–155, 1988a. 30614
- 10 McCartney, M. and Baxter, M.: Carbon-14 discharges from the nuclear fuel cycle: 2. Local effects, J. Environm. Radioactiv., 8, 157–171, 1988b. 30614
- Meesters, A., Tolk, L., Peters, W., Hutjes, R., Vellinga, O., Elbers, J., Vermeulen, A., Laan, S. V. D., Neubert, R., Meijer, H., and Dolman, A.: Inverse carbon dioxide flux estimates for the Netherlands, J. Geophys. Res.-Atmos., 117, D20306, doi:10.1029/2012JD017797, 2012. 30623
- 15 Meijer, H. A. J., Smid, H., Perez, E., and Keizer, M. G.: Isotopic characterisation of anthropogenic CO_2 emissions using isotopic and radiocarbon analysis, Phys. Chem. Earth, 21, 483–487, doi:10.1016/S0079-1946(97)81146-9, 1996. 30614
- Miller, J., Lehman, S., Montzka, S., Sweeney, C., Miller, B., Karion, A., Wolak, C., Dlugokencky, E., Southon, J., Turnbull, J., and Tans, P.: Linking emissions of fossil fuel CO_2 and other anthropogenic trace gases using atmospheric $^{14}\text{CO}_2$, J. Geophys. Res.-Atmos., 117, D08302, doi:10.1029/2011JD017048, 2012. 30613
- 20 Mlawer, E., Taubman, S., Brown, P., Iacono, M., and Clough, S.: Radiative transfer for inhomogeneous atmospheres: RRTM, a validated correlated- k model for the longwave, J. Geophys. Res.-Atmos., 102, 16663–16682, 1997. 30620
- 25 Mook, W. G. and van der Plicht, J.: Reporting ^{14}C activities and concentrations, Radiocarbon, 41, 227–239, 1999. 30613, 30619
- Naegler, T. and Levin, I.: Closing the global radiocarbon budget 1945–2005, J. Geophys. Res., 111, D12311, doi:10.1029/2005JD006758, 2006. 30614
- 30 Naegler, T. and Levin, I.: Observation-based global biospheric excess radiocarbon inventory 1963–2005, J. Geophys. Res.-Atmos., 114, D17302, doi:10.1029/2008JD011100, 2009a. 30617

Modeling $\Delta^{14}\text{CO}_2$ for
Western Europe

D. Bozhinova et al.

Title Page

Abstract

Introduction

Conclusions

References

Tables

Figures

◀

▶

◀

▶

Back

Close

Full Screen / Esc

Printer-friendly Version

Interactive Discussion



Naegler, T. and Levin, I.: Biosphere-atmosphere gross carbon exchange flux and the $\delta^{13}\text{CO}_2$ and $\Delta^{14}\text{CO}_2$ disequilibria constrained by the biospheric excess radiocarbon inventory, *J. Geophys. Res.-Atmos.*, 114, doi:10.1029/2008JD011116, 2009b. 30617

5 Nakanishi, M. and Niino, H.: An improved Mellor-Yamada level-3 model: its numerical stability and application to a regional prediction of advection fog, *Bound.-Lay. Meteorol.*, 119, 397–407, 2006. 30620

NCEP, US National Centers for Environmental Prediction: NCEP FNL Operational Model Global Tropospheric Analyses, continuing from July 1999, Dataset ds083.2 published by the CISL Data Support Section at the National Center for Atmos. Res., Boulder, CO, available at available at: <http://rda.ucar.edu/datasets/ds083.2/>, updated daily, 2013. 30619

10 Nydal, R.: Further investigation on the transfer of radiocarbon in nature, *J. Geophys. Res.*, 73, 3617–3635, 1968. 30614

Nydal, R. and Gislefoss, J.: Further application of bomb ^{14}C as a tracer in the atmosphere and ocean, *Radiocarbon*, 38, 389–406, 1996. 30614

15 Olivier, J. G. J. and Peters, J. A. H. W.: Uncertainties in global, regional and national emission inventories, in: *Non-CO₂ Greenhouse Gases: Scientific Understanding, Control Options and Policy Aspects*, edited by: van Ham, J., Baede, A. P. M., Guicherit, R., and Williams-Jacobse, J. F. G. M., Proceedings of the Third International Symposium, Maastricht, Netherlands, 21–23 January 2002, Millpress Science Publishers, Rotterdam, 525–540, ISBN 90-77017-70-4, 2002. 30613

20 Olsen, S. and Randerson, J.: Differences between surface and column atmospheric CO_2 and implications for carbon cycle research, *J. Geophys. Res.*, 109, D02301, doi:10.1029/2003JD003968, 2004. 30621

25 Palstra, S. W. L., Karstens, U., Streurman, H., and Meijer, H. A. J.: Wine ethanol ^{14}C as a tracer for fossil fuel CO_2 emissions in Europe: measurements and model comparison, *J. Geophys. Res.-Atmos.*, 113, D21305, doi:10.1029/2008JD010282, 2008. 30614, 30616, 30617

Peters, W., Krol, M. C., van der Werf, G. R., Houweling, S., Jones, C. D., Hughes, J., Schaefer, K., Masarie, K. A., Jacobson, A. R., Miller, J. B., Cho, C. H., Ramonet, M., Schmidt, M., Ciattaglia, L., Apadula, F., Helta, D., Meinhardt, F., di Sarra, A. G., Piacentino, S., Sferlazzo, D., Aalto, T., Hatakka, J., Strom, J., Haszpra, L., Meijer, H. A. J., Laan, S. V. D., Neubert, R. E. M., Jordan, A., Rodo, X., Morgui, J. A., Vermeulen, A. T., Popa, E., Rozanski, K., Zimnoch, M., Manning, A. C., Leuenberger, M., Uglietti, C., Dolman, A. J., Ciais, P., Heimann, M., and Tans, P. P.: Seven years of recent European net terrestrial carbon diox-

Modeling $\Delta^{14}\text{CO}_2$ for
Western Europe

D. Bozhinova et al.

Title Page

Abstract

Introduction

Conclusions

References

Tables

Figures

◀

▶

◀

▶

Back

Close

Full Screen / Esc

Printer-friendly Version

Interactive Discussion



ide exchange constrained by atmospheric observations, *Glob. Change Biol.*, 16, 1317–1337, doi:10.1111/j.1365-2486.2009.02078.x, 2010. 30620

Peylin, P., Houweling, S., Krol, M. C., Karstens, U., Rödenbeck, C., Geels, C., Vermeulen, A., Badawy, B., Aulagnier, C., Pregarer, T., Delage, F., Pieterse, G., Ciais, P., and Heimann, M.: Importance of fossil fuel emission uncertainties over Europe for CO_2 modeling: model intercomparison, *Atmos. Chem. Phys.*, 11, 6607–6622, doi:10.5194/acp-11-6607-2011, 2011. 30630

Pino, D., Vilà-Guerau de Arellano, J., Peters, W., Schröter, J., van Heerwaarden, C. C., and Krol, M. C.: A conceptual framework to quantify the influence of convective boundary layer development on carbon dioxide mixing ratios, *Atmos. Chem. Phys.*, 12, 2969–2985, doi:10.5194/acp-12-2969-2012, 2012. 30623, 30631

Pregarer, T., Scholz, Y., and Friedrich, R.: Documentation of the Anthropogenic GHG Emission Data for Europe Provided in the Frame of CarboEurope GHG and CarboEurope IP, Final Report CarboEurope-IP, Institute for Energy Economics and the Rational Use of Energy (IER), University of Stuttgart, Germany, 2007. 30621

Randerson, J., Enting, I., Schuur, E., Caldeira, K., and Fung, I. Y.: Seasonal and latitudinal variability of troposphere D^{14}CO_2 : Post bomb contributions from fossil fuels, oceans, the stratosphere, and the terrestrial biosphere, *Global Biogeochem. Cy.*, 16, 1112, doi:10.1029/2002GB001876, 2002. 30614

Raupach, M., Marland, G., Ciais, P., Quéré, C. L., Canadell, J., Klepper, G., and Field, C.: Global and regional drivers of accelerating CO_2 emissions, *P. Natl. Acad. Sci. USA*, 104, 10288–10293, doi:10.1073/pnas.0700609104, 2007. 30612

Riley, W., Hsueh, D., Randerson, J., Fischer, M. L., Hatch, J. G., Pataki, D. E., Wang, W., and Goulden, M. L.: Where do fossil fuel carbon dioxide emissions from California go? An analysis based on radiocarbon observations and an atmospheric transport model, *J. Geophys. Res.*, 113, G04002, doi:10.1029/2007JG000625, 2008. 30614, 30615, 30630

Schaefer, K., Collatz, G. J., Tans, P., Denning, A. S., Baker, I., Berry, J., Prihodko, L., Suits, N., and Philpott, A.: Combined simple biosphere/Carnegie–Ames–Stanford approach terrestrial carbon cycle model, *J. Geophys. Res.-Biogeo.*, 113, G03034, doi:10.1029/2007JG000603, 2008. 30620

Shibata, S., Kawano, E., and Nakabayashi, T.: Atmospheric $^{14}\text{CO}_2$ variations in Japan during 1982–1999 based on ^{14}C measurements of rice grains, *Appl. Radiat. Isotopes*, 63, 285–290, doi:10.1016/j.apradiso.2005.03.011, 2005. 30614

Modeling $\Delta^{14}\text{CO}_2$ for
Western Europe

D. Bozhinova et al.

Title Page

Abstract

Introduction

Conclusions

References

Tables

Figures

◀

▶

◀

▶

Back

Close

Full Screen / Esc

Printer-friendly Version

Interactive Discussion



- Skamarock, W., Klemp, J., Dudhia, J., Gill, D. O., Barker, D. M., Duda, M. G., Huang, X.-Y., Wang, W., and Powers, J. G.: A Description of the Advanced Research WRF Version 3. NCAR Technical Note NCAR/TN-475+STR, doi:10.5065/D68S4MVH, available at: <http://nldr.library.ucar.edu/repository/collections/TECH-NOTE-000-000-000-855>, 2008. 30619
- 5 Steeneveld, G.-J., Mauritsen, T., Bruijn, E. D., and de Arellano, J. V.-G.: Evaluation of limited-area models for the representation of the diurnal cycle and contrasting nights in CASES-99, *J. Appl. Meteorol. Clim.*, 47, 869–887, 2008. 30623, 30631
- Stuefer, M., Freitas, S. R., Grell, G., Webley, P., Peckham, S., McKeen, S. A., and Egan, S. D.: Inclusion of ash and SO_2 emissions from volcanic eruptions in WRF-Chem: development and some applications, *Geosci. Model Dev.*, 6, 457–468, doi:10.5194/gmd-6-457-2013, 2013. 10 30631
- Stuiver, M. and Polach, H.: Discussion: reporting of ^{14}C data, *Radiocarbon*, 19, 355–363, 1977. 30613, 30619
- Stuiver, M. and Quay, P.: Atmospheric ^{14}C changes resulting from fossil fuel CO_2 release and cosmic ray flux variability, *Earth Planet. Sci. Lett.*, 53, 349–362, 1981. 30614
- 15 Suess, H.: Radiocarbon concentration in modern wood, *Science*, 122, 415–417, 1955. 30614
- Tie, X., Madronich, S., Li, G., Ying, Z., Weinheimer, A., Apel, E., and Campos, T.: Simulation of Mexico City plumes during the MIRAGE-Mex field campaign using the WRF-Chem model, *Atmos. Chem. Phys.*, 9, 4621–4638, doi:10.5194/acp-9-4621-2009, 2009. 30631
- 20 Tolk, L. F., Peters, W., Meesters, A. G. C. A., Groenendijk, M., Vermeulen, A. T., Steeneveld, G. J., and Dolman, A. J.: Modelling regional scale surface fluxes, meteorology and CO_2 mixing ratios for the Cabauw tower in the Netherlands, *Biogeosciences*, 6, 2265–2280, doi:10.5194/bg-6-2265-2009, 2009. 30623
- Turnbull, J., Miller, J., Lehman, S., and Tans, P.: Comparison of $^{14}\text{CO}_2$, CO , and SF_6 as tracers for recently added fossil fuel CO_2 in the atmosphere and implications for biological CO_2 exchange, *Geophys. Res. Lett.*, 33, L01817, doi:10.1029/2005GL024213, 2006. 30613, 30616, 25 30617
- Turnbull, J. C., Miller, J. B., Lehman, S. J., Hurst, D., Peters, W., Tans, P. P., Southon, J., Montzka, S. A., Elkins, J. W., Mondeel, D. J., Romashkin, P. A., Elansky, N., and Skorokhod, A.: Spatial distribution of $\Delta^{14}\text{CO}_2$ across Eurasia: measurements from the TROICA-8 expedition, *Atmos. Chem. Phys.*, 9, 175–187, doi:10.5194/acp-9-175-2009, 2009a. 30618 30

Modeling $\Delta^{14}\text{CO}_2$ for Western Europe

D. Bozhinova et al.

Title Page

Abstract

Introduction

Conclusions

References

Tables

Figures

◀

▶

◀

▶

Back

Close

Full Screen / Esc

Printer-friendly Version

Interactive Discussion



- Turnbull, J., Rayner, P., Miller, J., Naegler, T., Ciais, P., and Cozic, A.: On the use of $^{14}\text{CO}_2$ as a tracer for fossil fuel CO_2 : Quantifying uncertainties using an atmospheric transport model, *J. Geophys. Res.*, 114, D22302, doi:10.1029/2009JD012308, 2009b. 30616, 30617
- Turnbull, J. C., Karion, A., Fischer, M. L., Faloona, I., Guilderson, T., Lehman, S. J., Miller, B. R., Miller, J. B., Montzka, S., Sherwood, T., Saripalli, S., Sweeney, C., and Tans, P. P.: Assessment of fossil fuel carbon dioxide and other anthropogenic trace gas emissions from airborne measurements over Sacramento, California in spring 2009, *Atmos. Chem. Phys.*, 11, 705–721, doi:10.5194/acp-11-705-2011, 2011. 30615
- van der Laan, S., Neubert, R. E. M., and Meijer, H. A. J.: A single gas chromatograph for accurate atmospheric mixing ratio measurements of CO_2 , CH_4 , N_2O , SF_6 and CO , *Atmos. Meas. Tech.*, 2, 549–559, doi:10.5194/amt-2-549-2009, 2009. 30624
- van der Laan, S., Karstens, U., Neubert, R., Laan-Luijckx, I. V. D., and Meijer, H.: Observation-based estimates of fossil fuel-derived CO_2 emissions in the Netherlands using ^{14}C , CO and ^{222}Rn , *Tellus B*, 62, 389–402, doi:10.1111/j.1600-0889.2010.00493.x, 2010. 30615, 30624, 30632
- van der Molen, M. and Dolman, A.: Regional carbon fluxes and the effect of topography on the variability of atmospheric CO_2 , *J. Geophys. Res.*, 112, D01104, doi:10.1029/2006JD007649, 2007. 30631
- van der Stricht, S. and Janssens, A.: Radioactive effluents from nuclear power stations and nuclear fuel reprocessing sites in the European Union, 2004–2008, *Radiation Protection*, 164, ISBN 978-92-79-16922-9, doi:10.2833/27366, 2010. 30621
- van Laar, H., Goudriaan, J., and Keulen, H. V.: SUCROS97: simulation of crop growth for potential and water-limited production situations; as applied to spring wheat, vol. 14, DLO Research Institute for Agrobiological and Soil Fertility and The C. T. de Wit Graduate School for Production Ecology, Wageningen University library, the Netherlands, available at: <http://edepot.wur.nl/4426>, 1997. 30622
- Vermeulen, A. T., Hensen, A., Popa, M. E., van den Bulk, W. C. M., and Jongejan, P. A. C.: Greenhouse gas observations from Cabauw Tall Tower (1992–2010), *Atmos. Meas. Tech.*, 4, 617–644, doi:10.5194/amt-4-617-2011, 2011. 30623
- Vilà-Guerau de Arellano, J., Gioli, B., Miglietta, F., Jonker, H. J. J., Baltink, H. K., Hutjes, R. W. A., and Holtslag, A. A. M.: Entrainment process of carbon dioxide in the atmospheric boundary layer, *J. Geophys. Res.*, 109, D18110, doi:10.1029/2004JD004725, 2004. 30623, 30631

Vogel, F., Hammer, S., Steinhof, A., Kromer, B., and Levin, I.: Implication of weekly and diurnal ^{14}C calibration on hourly estimates of CO-based fossil fuel CO₂ at a moderately polluted site in southwestern Germany, *Tellus B*, 62, 512–520, 2010. 30615

Vogel, F., Tiruchittampalam, B., Theloke, J., Kretschmer, R., Gerbig, C., Hammer, S., and Levin, I.: Can we evaluate a fine-grained emission model using high-resolution atmospheric transport modelling and regional fossil fuel CO₂ observations?, *Tellus B*, 65, 18681, doi:10.3402/tellusb.v65i0.18681, 2013. 30615, 30632

Wang, Z., Xiang, Y., and Guo, Q.: ^{14}C levels in tree rings located near Qinshan Nuclear Power Plant, China, *Radiocarbon*, 54, doi:10.2458/azu_js_rc.v54i2.15869, 2012. 30614

Wang, Z., Xiang, Y., and Guo, Q.: Terrestrial distribution of ^{14}C in the vicinity of Qinshan nuclear power plant, China, *Radiocarbon*, 55, 59–66, 2013. 30614

Watson, A. J., Schuster, U., Bakker, D. C. E., Bates, N. R., Corbiere, A., Gonzalez-Davila, M., Friedrich, T., Hauck, J., Heinze, C., Johannessen, T., Kortzinger, A., Metzl, N., Olafsson, J., Olsen, A., Oschlies, A., Padin, X. A., Pfeil, B., Santana-Casiano, J. M., Steinhoff, T., Telszewski, M., Rios, A. F., Wallace, D. W. R., and Wanninkhof, R.: Tracking the variable North Atlantic sink for atmospheric CO₂, *Science*, 326, 1391–1393, doi:10.1126/science.1177394, 2009. 30617

Willmott, C.: Some comments on the evaluation of model performance, *B. Am. Meteorol. Soc.*, 63, 1309–1313, 1982. 30623, 30644

ACPD

13, 30611–30652, 2013

Modeling $\Delta^{14}\text{CO}_2$ for Western Europe

D. Bozhinova et al.

Title Page

Abstract

Introduction

Conclusions

References

Tables

Figures

◀

▶

◀

▶

Back

Close

Full Screen / Esc

Printer-friendly Version

Interactive Discussion



Table 1. The observational sites with data used in this study and statistics for the daily concentrations of CO_2 and $\text{CO}_{2\text{ff}}$ estimated from CO observations, hourly flux CO_2 and monthly integrated $\Delta^{14}\text{CO}_2$ observations as compared with modeled results. Here $\overline{\text{Pi}} - \overline{\text{Oi}}$ represents the mean model-data difference, $\sigma_{\text{Pi}-\text{Oi}}$ – the spread of the difference, both of which carry the units described in the header of each section, while r – the Pearson's coefficient of correlation and d – the coefficient of determination (Willmott, 1982) are dimensionless measures and n – number of members for the statistical analysis.

Site	Latitude [° N]	Longitude [° E]	Elevation [m]	Altitude [m]	Owner	Provider	$\overline{\text{Pi}} - \overline{\text{Oi}}$	$\sigma_{\text{Pi}-\text{Oi}}$	r	d	n
CO ₂ concentration [ppm]											
Cabauw, NL	51.97	4.93	0.7	20	ECN, NL ^a	CarboEurope IP ^b	5.58	8.19	0.64	0.72	185
Cabauw, NL	51.97	4.93	0.7	60	ECN, NL	CarboEurope IP	3.69	6.37	0.65	0.74	185
Cabauw, NL	51.97	4.93	0.7	120	ECN, NL	CarboEurope IP	2.76	5.48	0.67	0.77	185
Cabauw, NL	51.97	4.93	0.7	200	ECN, NL	CarboEurope IP	1.40	4.50	0.74	0.84	185
Heidelberg, DE	49.42	8.67	116	30	IUP-UHEI, DE ^c	CarboEurope IP	4.29	7.31	0.69	0.77	185
Loobos, NL	52.17	5.74		24.5	Alterra-WUR, NL ^d	CarboEurope IP	3.82	6.90	0.59	0.71	185
Lutjewad, NL	53.40	6.36	3	60	CIO-RUG, NL ^e	CIO-RUG, NL	-0.60	7.43	0.53	0.73	167
Lutjewad, NL – CO _{2ff}	53.40	6.36	3	60	CIO-RUG, NL	CIO-RUG, NL	-3.29	3.64	0.66	0.69	166
Neuglobsow, DE	53.17	13.03	65		UBA, DE ^f	WDCGG ^g	-2.31	8.62	0.58	0.74	185
Schauinsland, DE – 5 min	47.92	7.92	1200	7	UBA, DE	WDCGG	0.20	4.13	0.81	0.89	153
Schauinsland, DE – conti	47.92	7.92	1200	7	UBA, DE	WDCGG	0.17	3.59	0.85	0.92	177
Sonnblick, AT	47.05	12.95	3106		EEA, AT ^h	WDCGG	1.57	2.74	0.86	0.88	185
Zugspitze, DE	47.42	10.98	2656		UBA, DE	WDCGG	0.79	3.07	0.82	0.88	161
CO ₂ surface flux [mg CO ₂ m ⁻² s ⁻¹]											
Cabauw, NL	51.97	4.93	0.7	1	KNMI, NL ⁱ	CESAR ^j	-0.01	0.26	0.70	0.83	2662
$\Delta^{14}\text{CO}_2$ integrated sample [‰]											
Jungfraujoch, CH	46.55	8.00	3450	5	IUP-UHEI, DE	IUP-UHEI, DE	1.05	1.61	0.71	0.74	6
Lutjewad, NL	53.40	6.36	3	60	CIO-RUG, NL	CIO-RUG, NL	8.82	5.16	-0.87	0.12	6
Schauinsland, DE	47.92	7.92	1200	7	IUP-UHEI, DE	IUP-UHEI, DE	-1.89	1.83	0.74	0.75	6

^a ECN – Energy Research Center of the Netherlands, the Netherlands; contact person – Alex Vermeulen, a.vermeulen@ecn.nl

^b CarboEuropeIP – CarboEurope Integrated Project; <http://www.carboeurope.org>

^c IUP-UHEI – Institute of Environmental Physics, University of Heidelberg, Germany; contact person – Dr. Ingeborg Levin, Ingeborg.Levin@iup.uni-heidelberg.de

^d Alterra-WUR – Alterra, Wageningen University, the Netherlands; contact person – Dr. ir. Eddy Moors, eddy.moors@wur.nl

^e CIO-RUG – Center for Isotope Research, University of Groningen, the Netherlands; contact person – Prof.dr. Harro Meijer, H.A.J.Meijer@rug.nl

^f UBA, DE – Federal Environmental Agency, Germany; contact person – Karin Uhse, karin.uhse@uba.de

^g WDCGG – World Data Center for Greenhouse Gases; <http://ds.data.jma.go.jp/gmd/wdogg/>

^h EEA, AT – Environmental Agency Austria, Austria; contact person – Marina Fröhlich, marina.froehlich@umweltbundesamt.at

ⁱ KNMI – Royal Netherlands Meteorological Institute, the Netherlands; contact person – Dr. Fred Bosveld, Fred.Bosveld@knmi.nl

^j CESAR – Cabauw Experimental Site for Atmospheric Research, the Netherlands; <http://www.cesar-observatory.nl>

Title Page

Abstract

Introduction

Conclusions

References

Tables

Figures

◀

▶

◀

▶

Back

Close

Full Screen / Esc

Printer-friendly Version

Interactive Discussion



Modeling $\Delta^{14}\text{CO}_2$ for Western Europe

D. Bozhinova et al.

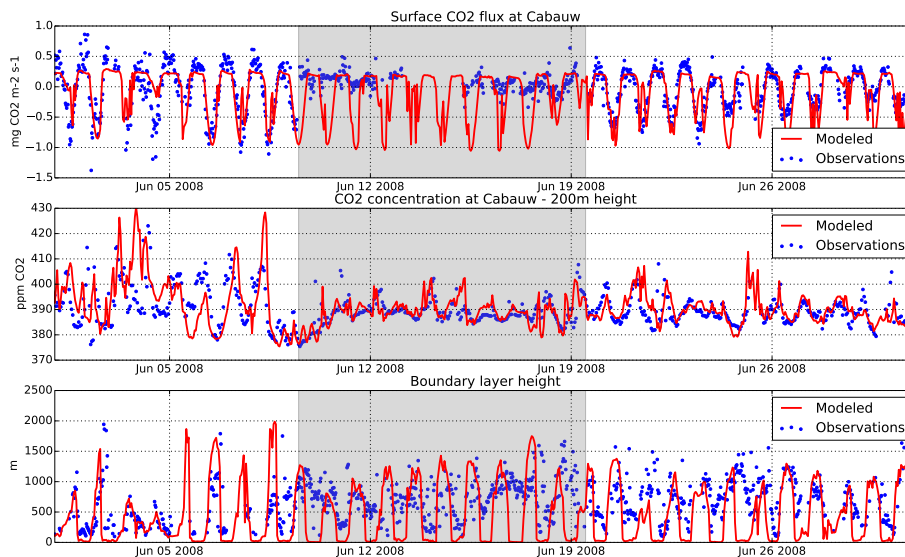


Fig. 1. Comparison between modeled and observed CO_2 fluxes, concentrations and boundary layer height for the location of Cabauw for one month in the simulated season. Performance is usually better on clear days as compared to cloudy ones, indicated in the graph with the gray background.

[Title Page](#)[Abstract](#)[Introduction](#)[Conclusions](#)[References](#)[Tables](#)[Figures](#)[◀](#)[▶](#)[◀](#)[▶](#)[Back](#)[Close](#)[Full Screen / Esc](#)[Printer-friendly Version](#)[Interactive Discussion](#)

Modeling $\Delta^{14}\text{CO}_2$ for Western Europe

D. Bozhinova et al.

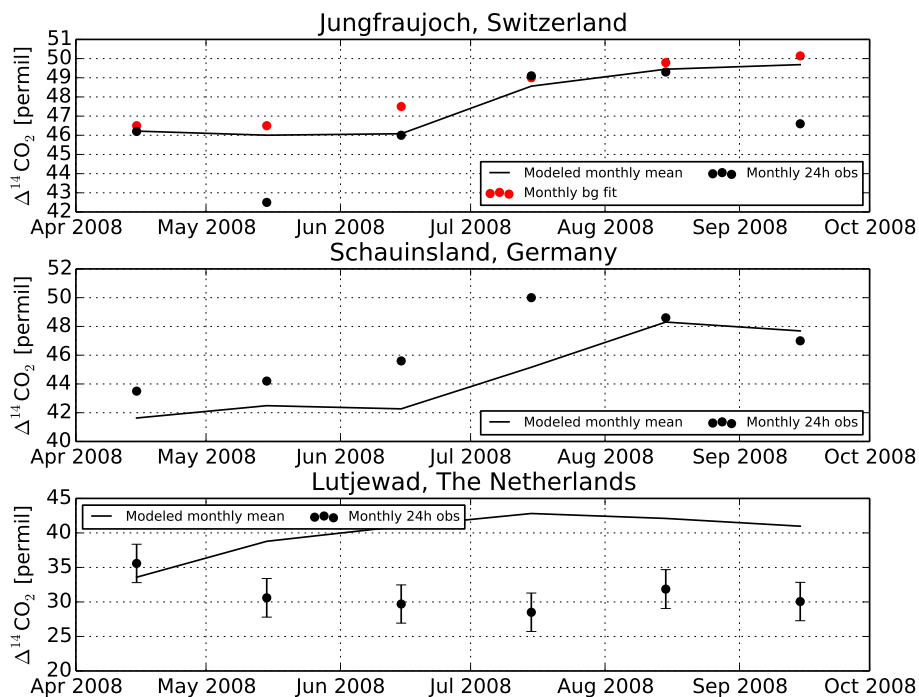


Fig. 2. Comparison between monthly observed and modeled atmospheric $\Delta^{14}\text{CO}_2$ integrated samples for (a) Jungfrauoch, Switzerland, (b) Schauinsland, Germany and (c) Lutjewad, the Netherlands. In (a) with red circles are shown the monthly fit values used for the signature of the background CO_2 (Δ_{bg}) in our calculations.

Modeling $\Delta^{14}\text{CO}_2$ for Western Europe

D. Bozhinova et al.

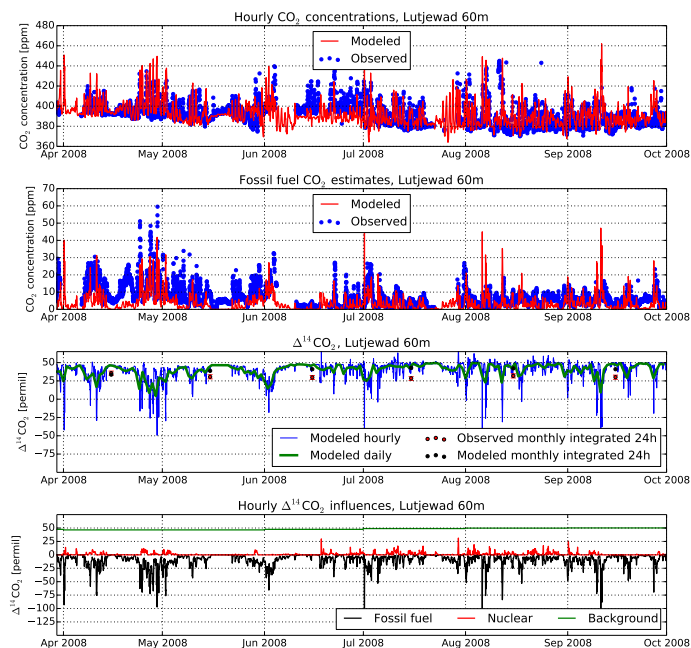


Fig. 3. 6 months of hourly results for Lutjewad at 60 m height. Comparison between observed and modeled (a) CO_2 concentrations, (b) $\text{CO}_{2\text{ff}}$ concentrations (c) atmospheric $\Delta^{14}\text{CO}_2$ and (d) the contribution of different compounds for the resulting $\Delta^{14}\text{CO}_2$. The variations in the $\Delta^{14}\text{CO}_2$ signal are directly connected with the transport of fossil fuel CO_2 enriched air at the location, but are not captured by current observations due to their low temporal resolution.

Modeling $\Delta^{14}\text{CO}_2$ for Western Europe

D. Bozhinova et al.

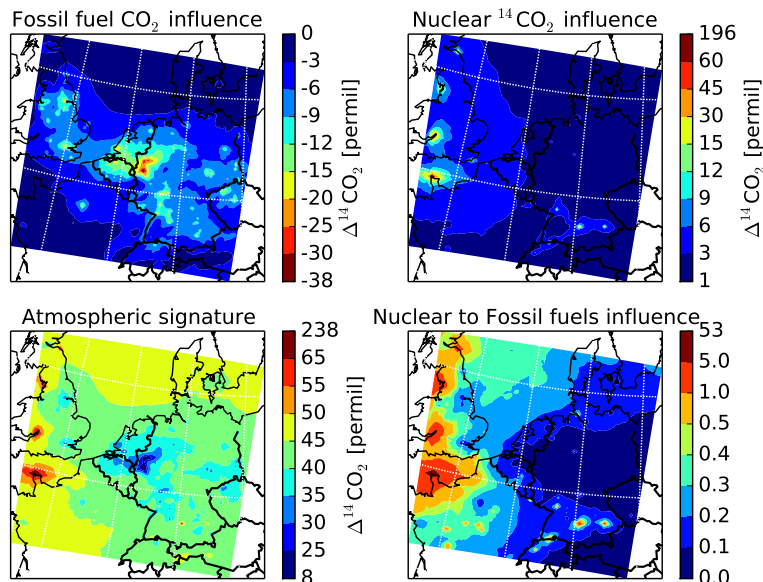


Fig. 4. Spatial distribution for the 6 month averaged (a) fossil fuel CO_2 emissions influence, (b) nuclear $^{14}\text{CO}_2$ emissions influence, (c) resulting $\Delta^{14}\text{CO}_2$ signature in the atmosphere and (d) the ratio between the nuclear and fossil fuel influences on the atmospheric signature, all averaged over the lower 1200 m of the atmosphere. While the biggest influence over Europe for changes in the $\Delta^{14}\text{CO}_2$ in the atmosphere is of fossil fuel CO_2 , the effect of the nuclear emissions of $^{14}\text{CO}_2$ can be of comparable magnitude for large areas in France and UK.

Title Page

Abstract

Introduction

Conclusions

References

Tables

Figures

◀

▶

◀

▶

Back

Close

Full Screen / Esc

Printer-friendly Version

Interactive Discussion

Modeling $\Delta^{14}\text{CO}_2$ for
Western Europe

D. Bozhinova et al.

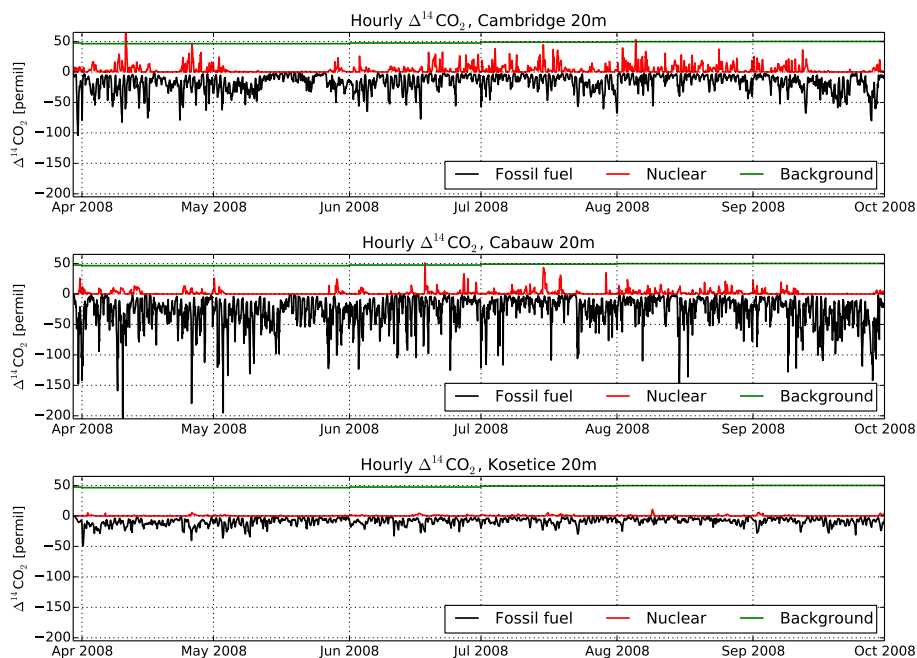


Fig. 5. Time series for the relative importance of nuclear vs. fossil fuel influence on the resulting atmospheric $\Delta^{14}\text{CO}_2$ for three locations in our domain – near Cambridge (UK), Cabauw (the Netherlands) and Kosetice (Czech Republic).

Title Page

Abstract

Introduction

Conclusions

References

Tables

Figures

◀

▶

◀

▶

Back

Close

Full Screen / Esc

Printer-friendly Version

Interactive Discussion



Modeling $\Delta^{14}\text{CO}_2$ for
Western Europe

D. Bozhinova et al.

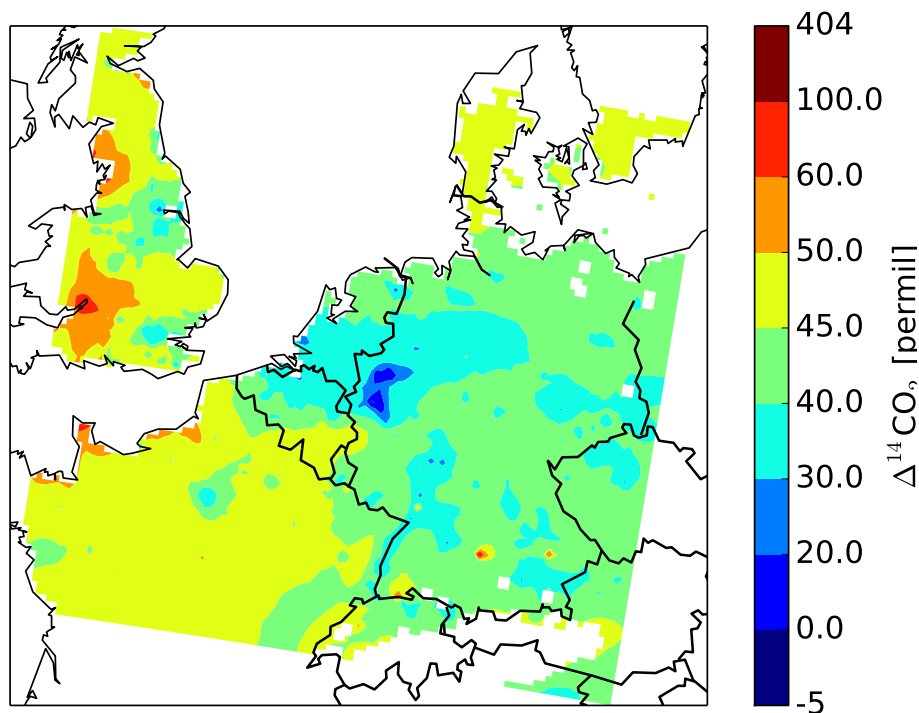


Fig. 6. Modeled absolute $\Delta^{14}\text{CO}_2$ signature of maize leaves at flowering. Both the highly industrialized areas in Germany, where the atmospheric $\Delta^{14}\text{CO}_2$ is lower than the background, and the enriched areas near the big nuclear sources in France and UK are visible also in the plants. Even on this resolution we see in the plant signature the hotspots around Paris, London, Frankfurt, and many other big cities.

[Title Page](#)[Abstract](#)[Introduction](#)[Conclusions](#)[References](#)[Tables](#)[Figures](#)[◀](#)[▶](#)[◀](#)[▶](#)[Back](#)[Close](#)[Full Screen / Esc](#)[Printer-friendly Version](#)[Interactive Discussion](#)

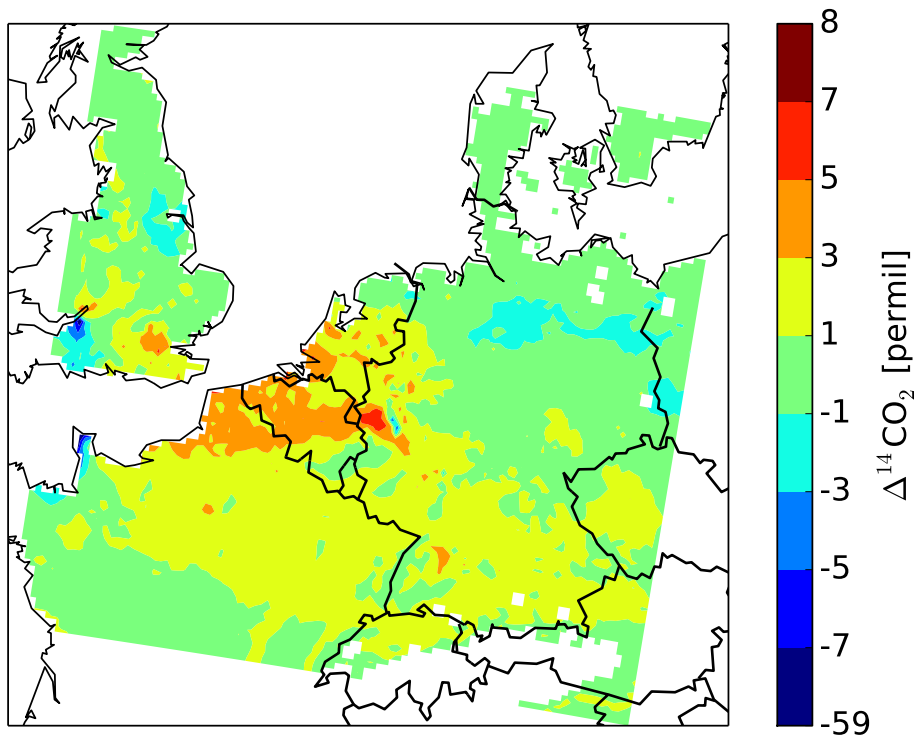


Fig. 7. Difference between $\Delta^{14}\text{CO}_2$ modeled in plants and the atmospheric average. This figure shows the covariance between the plant growth and the variability in the atmospheric $\Delta^{14}\text{CO}_2$, which in essence is the error that should be expected if the plant growth is not taken into account and the plant signature is assumed to be equal to the atmospheric average.

Modeling $\Delta^{14}\text{CO}_2$ for Western Europe

D. Bozhinova et al.

Title Page

Abstract Introduction

Conclusions References

Tables Figures

◀ ▶

◀ ▶

Back Close

Full Screen / Esc

Printer-friendly Version

Interactive Discussion



Modeling $\Delta^{14}\text{CO}_2$ for Western Europe

D. Bozhinova et al.

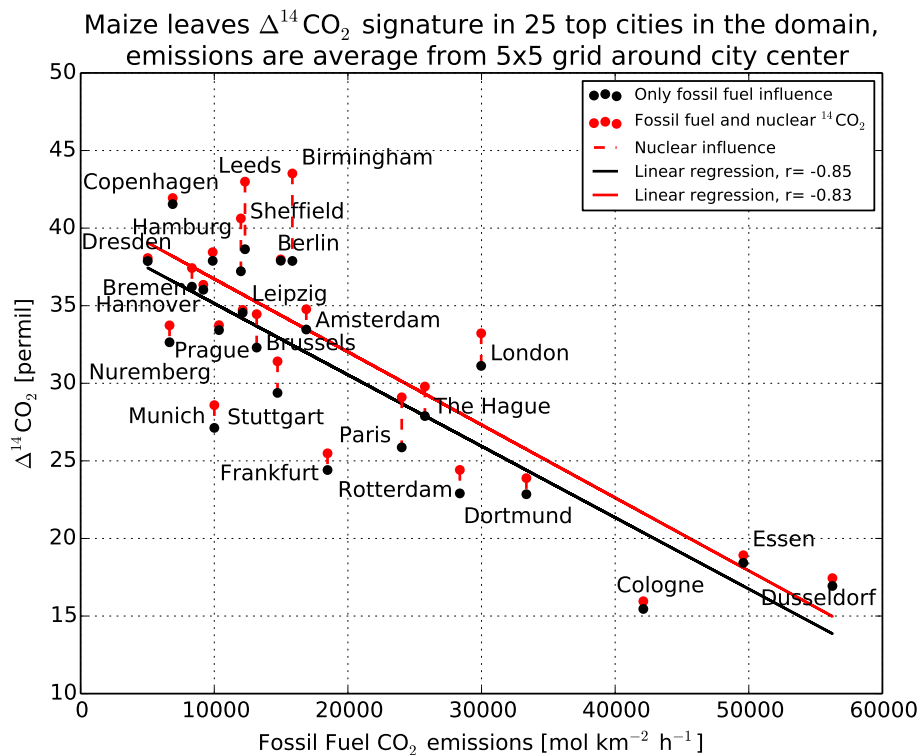


Fig. 8. Regional scale comparison between the modeled maize leaves $\Delta^{14}\text{CO}_2$ signature at city center and fossil fuel CO_2 emissions averaged for 5×5 grid around the city center on 12 km horizontal resolution.

Title Page

Abstract

Introduction

Conclusions

References

Tables

Figures

◀

▶

◀

▶

Back

Close

Full Screen / Esc

Printer-friendly Version

Interactive Discussion

